■ **Solid-State Structures** │*Hot Paper*│

Crystalline Nitridophosphates by Ammonothermal Synthesis

Mathias Mallmann, Sebastian Wendl, and Wolfgang Schnick*[a]

Abstract: Nitridophosphates are a well-studied class of compounds with high structural diversity. However, their synthesis is quite challenging, particularly due to the limited thermal stability of starting materials like P_3N_5. Typically, it requires even high-pressure techniques (e.g. multianvil) in most cases. Herein, we establish the ammonothermal method as a versatile synthetic tool to access nitridophosphates with different degrees of condensation. α-$Li_{10}P_4N_{10}$, β-$Li_{10}P_4N_{10}$, $Li_{18}P_6N_{16}$, Ca_2PN_3, SrP_8N_{14}, and $LiPN_2$ were synthesized in supercritical NH_3 at temperatures and pressures up to 1070 K and 200 MPa employing ammonobasic conditions. The products were analyzed by powder X-ray diffraction, energy dispersive X-ray spectroscopy, and FTIR spectroscopy. Moreover, we established red phosphorus as a starting material for nitridophosphate synthesis instead of commonly used and not readily available precursors, such as P_3N_5. This opens a promising preparative access to the emerging compound class of nitridophosphates.

Introduction

By analogy with well-known hydrothermal syntheses, the ammonothermal method was developed by Jacobs and co-workers and was established as an innovative synthetic approach for amides, imides and nitrides.[1–5] The ammonothermal technique gained fundamental interest in materials science as it facilitates the growth of high-quality GaN single crystals up to 50 mm in diameter with growth rates of several hundred μm per day.[6–9]

Recent explorative syntheses under ammonothermal conditions made crystalline wurtzite-type Grimm–Sommerfeld analogous nitrides available, such as InN, II-IV-N_2 compounds (II = Mg, Mn, Zn; IV = Si, Ge) and $CaGaSiN_3$, as well as oxide nitride perovskites such as $LnTaON_2$ (Ln = La, Ce, Pr, Nd, Sm, Gd).[10–15] Applying the ammonothermal technique, even the challenging preparation of a few nitridophosphates has been accomplished successfully as reported for $K_3P_6N_{11}$ and the double nitrides Mg_2PN_3 and Zn_2PN_3.[16–18] Furthermore, various phosphorus-containing imidonitrides were synthesized in supercritical ammonia and thus, the ammonothermal method appears as a promising general synthetic approach for nitridophosphate synthesis.[19–22]

Nitridophosphates are built up from PN_4 tetrahedra and their tetrahedra-based networks can be characterized by the degree of condensation $\kappa = n(T)/n(X)$, which represents the atomic ratio of tetrahedral centers (T = P) and coordinating atoms (X = N). Accordingly, compounds that are built up from non-condensed PN_4 tetrahedra (e.g. Li_7PN_4)[23] possess a degree of condensation of $\kappa = 1/4$, whereas highly condensed frameworks feature $\kappa \geq 1/2$ (e.g. $LiPN_2$).[24] For $1/4 < \kappa < 1/2$, partially condensed PN_4 tetrahedra may form complex anions, such as adamantane-like groups (α-$Li_{10}P_4N_{10}$, β-$Li_{10}P_4N_{10}$),[25,26] chain structures (e.g. Ca_2PN_3),[27] or layers (e.g. $Ho_2P_3N_7$).[28] The degree of condensation may further be correlated with materials properties, such as chemical inertness and rigidity of the network as well as physical properties like ion conductivity.[18] Nitridophosphate synthesis, however, is a challenging issue, as these compounds are prone to thermal decomposition starting at 1020 K and the elimination of N_2 at elevated temperatures [Eq. 1]:

$$P_3N_5 \rightarrow 3\,PN + N_2 \rightarrow 3\,P + 5/2\,N_2 \qquad (1)$$

Consequently, the number of nitridophosphates synthesized at ambient pressure so far is limited (e.g. Ca_2PN_3, α-$Li_{10}P_4N_{10}$, β-$Li_{10}P_4N_{10}$, $LiPN_2$ or Mg_2PN_3).[24–27,29] Following Le Chatelier's principle, thermal decomposition, however, can be suppressed by applying pressure. In this context, especially the multianvil technique ($p \leq 25$ GPa) turned out to be a powerful synthetic tool.[18] This high-pressure high-temperature method revealed numerous nitridophosphates with different types of anionic tetrahedra-based networks (e.g. SrP_8N_{14}, $Li_{18}P_6N_{16}$ or $LiNdP_4N_8$).[30–32] Nevertheless, utilizing high-pressure techniques implicates small sample volumes, which limits detailed characterization of materials properties as well as practical applications. Furthermore, precursors like P_3N_5 are typically used,[18] requiring a multistep synthesis procedure. Thus, the ammono-

[a] M. Mallmann, S. Wendl, Prof. Dr. W. Schnick
Department of Chemistry, University of Munich (LMU)
Butenandtstraße 5–13 (D), 81377 Munich (Germany)
E-mail: wolfgang.schnick@uni-muenchen.de

Supporting information and the ORCID identification number(s) for the author(s) of this article can be found under:
https://doi.org/10.1002/chem.201905227.

thermal method is a promising and innovative alternative, as it enables the preparation of large-volume samples, while suppressing thermal decomposition by medium pressures ($p \leq$ 300 MPa). However, there has been no systematic investigation on the ammonothermal synthesis of nitridophosphates that covers their broad structural diversity.

In this contribution, we exemplarily present the ammonothermal synthesis ($T \leq$ 1070 K, $p \leq$ 200 MPa) of six nitridophosphates that feature non-condensed PN_4 tetrahedra groups, infinite PN_4 tetrahedra chains, layered substructures, and highly condensed frameworks, namely α-$Li_{10}P_4N_{10}$, β-$Li_{10}P_4N_{10}$, $Li_{18}P_6N_{16}$, Ca_2PN_3, SrP_8N_{14}, and $LiPN_2$. This is a major extension of the structural diversity of ammonothermally accessible ternary and multinary compounds, which have hitherto been limited mainly to wurtzite-type derivatives and oxide nitride perovskites. In addition, red phosphorus (P_{red}), which was up to now only used for the synthesis of HPN_2 in ammonia,[33] is employed as a starting material for nitridophosphates. This makes highly reactive and chlorine-containing precursors (e.g. PCl_5, $(PNCl_2)_3$) dispensable, which can produce toxic and corrosive byproducts, emphasizing the innovative character of the ammonothermal approach.

Results and Discussion

Ammonothermal synthesis

Nitridophosphates α-$Li_{10}P_4N_{10}$, β-$Li_{10}P_4N_{10}$, $Li_{18}P_6N_{16}$, Ca_2PN_3, SrP_8N_{14}, and $LiPN_2$ were synthesized ammonothermally using custom-built high-pressure, high-temperature autoclaves. P_3N_5 or P_{red} were used as phosphorus source during syntheses. The other starting materials as well as the corresponding reaction conditions (maximum reaction temperature T_{max}, maximum pressure p_{max}, reaction time at maximum temperature t) are summarized in Table 1. Ammonobasic mineralizers, such as alkali metals, alkali metal nitrides, alkali metal azides or alkaline earth metal azides, which react in situ to the corresponding metal amides, were added to increase the solubility of the starting materials by forming soluble intermediate species. Since such intermediates are preferentially formed at lower temperatures, an additional temperature step at 670 K (holding time: 16 h) was conducted for all reactions before heating to T_{max}.[5] The addition of these mineralizers can also dissolve compounds such as P_{red}, which are actually insoluble in NH_3 even

at temperatures above the critical point.[34] Therefore, in the case of the synthesized lithium nitridophosphates (α-$Li_{10}P_4N_{10}$, β-$Li_{10}P_4N_{10}$, $Li_{18}P_6N_{16}$ and $LiPN_2$), Li_3N or Li was added, respectively, in excess to increase the solubility of P_{red}. While NaN_3 was added for the synthesis of Ca_2PN_3, to increase both, the solubility of Ca and P_{red}, no additional mineralizer was added for the synthesis of SrP_8N_{14}. Instead, $Sr(N_3)_2$ acts as an ammonobasic mineralizer itself by forming $Sr(NH_2)_2$, as the heavier alkaline earth metals have been discussed as ammonobasic mineralizers as well.[35] Possible intermediates are mixed-metal amides, such as $NaCa(NH_2)_3$, and reactive P/N compounds, for example, hexaaminocyclotriphosphazene $(PN(NH_2)_2)_3$, the corresponding ammoniate $(PN(NH_2)_2)_3 \cdot 0.5 NH_3$ or imidonitrides in analogy to $Na_{10}[P_4(NH)_6N_4](NH_2)_6(NH_3)_{0.5}$, which have already been synthesized using the ammonothermal method.[20,36–38] A possible condensation mechanism of phosphorus containing intermediates is illustrated in Scheme 1. When starting from
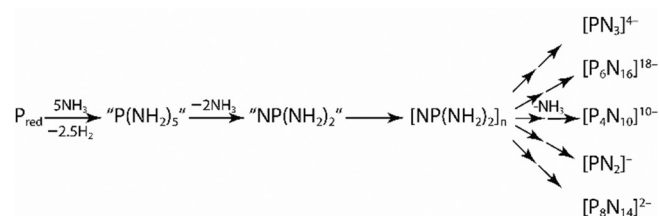
Scheme 1. Simplified condensation sequence of nitridophosphates during ammonothermal synthesis, starting from P_{red}.

P_{red}, the element has to be oxidized in a first step to an oxidation state of +V forming an intermediate species like hypothetical „$P(NH_2)_5$", in which two possible mechanisms are conceivable. On the one hand, N_2, which originates from the decomposition of NH_3, could act as oxidizing agent, on the other hand, NH_3 could directly react with P_{red} under elimination of H_2. „$P(NH_2)_5$" could immediately form „$NP(NH_2)_2$" by elimination of ammonia, which can react to reactive P/N compounds such as $(PN(NH_2)_2)_3$.[37] However, for a precise statement on possible reaction mechanisms or phosphorus containing intermediates, in situ measurements like Raman or NMR spectroscopy could be helpful.

Subsequent heating from 670 K to the maximum temperature T_{max} (see Table 1) leads to decomposition of the discussed intermediates and formation of the corresponding nitridophosphates under elimination of NH_3 (see Scheme 1). After reaction, residual mineralizers and intermediate species were removed by washing of the products with dry ethanol (α-$Li_{10}P_4N_{10}$, β-$Li_{10}P_4N_{10}$, $Li_{18}P_6N_{16}$, and Ca_2PN_3) or 1 M HCl (SrP_8N_{14} and $LiPN_2$). SEM images of octahedrally shaped β-$Li_{10}P_4N_{10}$ and needle-shaped SrP_8N_{14} crystallites are illustrated in Figure 1, while the other compounds were obtained as microcrystalline powders.

As mentioned above, both P_3N_5 and P_{red} were used as starting materials. While α-$Li_{10}P_4N_{10}$, β-$Li_{10}P_4N_{10}$, Ca_2PN_3, and $LiPN_2$ were synthesized starting from P_{red}, $Li_{18}P_6N_{16}$ and SrP_8N_{14} could only be obtained starting from P_3N_5. A possible explanation could be the higher reactivity of P_3N_5 compared to P_{red}, which is needed for the synthesis of $Li_{18}P_6N_{16}$ and SrP_8N_{14}.[24–27,30,31]

Table 1. Starting materials, mineralizers and reaction conditions of the ammonothermal synthesis of α-$Li_{10}P_4N_{10}$, β-$Li_{10}P_4N_{10}$, $Li_{18}P_6N_{16}$, Ca_2PN_3, SrP_8N_{14}, and $LiPN_2$.

Compd.	Starting materials	Mineralizer	T_{max} [K]	p_{max} [MPa]	t [h]
α-$Li_{10}P_4N_{10}$	$Li_3N + P_{red}$	Li_3N	920	100	72
β-$Li_{10}P_4N_{10}$	$Li_3N + P_{red}$	Li_3N	1070	135	72
$Li_{18}P_6N_{16}$	$Li_3N + P_3N_5$	Li_3N	970	165	50
Ca_2PN_3	$CaH_2 + P_{red}$	NaN_3	870	200	96
SrP_8N_{14}	$Sr(N_3)_2 + P_3N_5$	$Sr(N_3)_2$	1070	170	96
$LiPN_2$	$Li + P_{red}$	Li	1070	135	96

Figure 1. SEM images of octahedrally shaped crystals of β-$Li_{10}P_4N_{10}$ (a) and crystalline needles of SrP_8N_{14} (b).

Probably, higher synthesis temperatures and pressures would lead to successful synthesis of these two compounds starting from P_{red} as well.

The introduction of P_{red} as a starting material for nitridophosphate synthesis as well as the use of simple starting materials like pure elements, lower reaction temperatures, pressures and larger sample volumes compared to other synthesis methods, indicates the high potential of the ammonothermal approach as an alternative synthetic tool for a systematic access to nitridophosphates.

Crystallographic investigation

The purified products were analyzed by PXRD. Rietveld refinements of α-$Li_{10}P_4N_{10}$, β-$Li_{10}P_4N_{10}$, $Li_{18}P_6N_{16}$, Ca_2PN_3, and $LiPN_2$ were conducted starting from atomic coordinates and Wyckoff positions known from the literature.[24–27,31] An exemplary Rietveld plot of Ca_2PN_3 is illustrated in Figure 2. The Rietveld plots of α-$Li_{10}P_4N_{10}$, β-$Li_{10}P_4N_{10}$, $Li_{18}P_6N_{16}$, and $LiPN_2$ can be found in the Supporting Information (Figures S1 and S6, Supporting Information). The crystallographic data as well as atomic coordinates are summarized in Tables S1–S4, S6–7 and S10–11 in the Supporting Information. In the case of $Li_{18}P_6N_{16}$ additional reflections could be observed, which can be attributed to α-$Li_{10}P_4N_{10}$ and $LiPN_2$. Due to the fact that $Li_{18}P_6N_{16}$ is so far only reported using high-pressure conditions (1270 K, 5.5 GPa), a
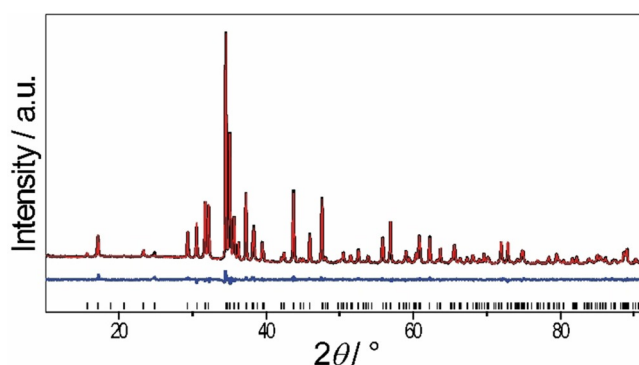

Figure 2. Rietveld refinement of PXRD pattern ($\lambda = 1.5406$ Å) of Ca_2PN_3 with experimental data (black line), calculated data (red line), difference profile (blue line) and reflection positions (black bars). Start values for Rietveld refinement were taken from literature.[27] Unknown reflections between 6 and 10° only occur after washing treatment and were, therefore, not taken into account during the refinement.

possible explanation for these side phases could be that higher reaction pressures would be necessary to achieve phase purity.[31] In analogy, higher pressures as well as temperatures would be necessary for the synthesis of SrP_8N_{14}, as the synthesis at 1070 K and 170 MPa resulted in broad reflections in the measured PXRD pattern (see Figure S5 in the Supporting Information), suggesting a nanocrystalline sample morphology. However, further increases of temperature or pressure are challenging and not possible with the current high-pressure equipment. Therefore, the measured PXRD was only compared with a simulated pattern from literature data (see Figure S5, Supporting Information)[30] and may most likely be characterized as SrP_8N_{14}.

EDX measurements of all compounds are summarized in Tables S5, S8, S9, and S12 in the Supporting Information. Deviations from the theoretical values can be explained by surface hydrolysis during sample preparation, washing treatment or by crystalline and amorphous side phases. The absence of any NH_x functionality in the Li containing nitridophosphates was confirmed by FTIR spectroscopy (Figures S2–S4 and S7 in the Supporting Information).

Crystal structures

α-$Li_{10}P_4N_{10}$, β-$Li_{10}P_4N_{10}$, and $Li_{18}P_6N_{16}$ are built up from corner sharing PN_4 tetrahedra. While α-$Li_{10}P_4N_{10}$ and β-$Li_{10}P_4N_{10}$ contain adamantane-like T2 supertetrahedra ($[P_4N_{10}]^{10-}$) with a degree of condensation of $\kappa = 2/5$, $Li_{18}P_6N_{16}$ is built up from $[P_6N_{16}]^{18-}$ anions corresponding to a degree of condensation of $\kappa = 3/8$ (see Figure 3). These $[P_6N_{16}]^{18-}$ units consist of four PN_4 tetrahedra forming a *vierer*-ring, which is connected to two further PN_4 tetrahedra forming two *dreier*-rings.[39,40] In contrast to these non-condensed tetrahedra groups, the anionic P/N-structure of Ca_2PN_3 is composed of *zweier* single chains running along [100] made up of corner sharing PN_4 tetrahedra (see Figure 3).[39,40] The chains exhibit a stretching factor of $f_s = 1.0$ and a degree of condensation of $\kappa = 1/3$. The crystal structure of SrP_8N_{14} is composed of PN_4 tetrahedra forming a layered structure (see Figure 3) and can be described as a highly condensed nitridophosphate with a degree of condensation of $\kappa = 4/7$. This is the highest degree of condensation observed in nitridophosphates so far. $LiPN_2$ is composed of all-side vertex-sharing PN_4 tetrahedra, which are connected via common corners forming a 3D anionic network with a degree of condensation of $\kappa = 1/2$ (see Figure 3) isoelectronic and homeotypic to β-cristobalite (SiO_2). Detailed crystal structure descriptions of all six compounds are given in the literature.[24–27,30,31] As shown in Figure 3, the above described nitridophosphates can be divided into different groups regarding their anionic P/N-substructures (non-condensed tetrahedra groups, tetrahedra chains, tetrahedra layers, and tetrahedra networks). This is a major extension of the structural diversity of ammonothermally accessible ternary and multinary nitrides, which have hitherto been limited mainly to wurtzite-type derivatives and oxide nitride perovskites. Furthermore, the degree of condensation of ammonothermally accessible nitridophosphates is widely extended and ranges now from $\kappa = 1/3$ to 4/7 (see Figure 4), cov-
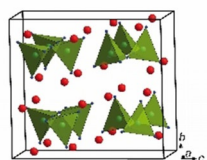
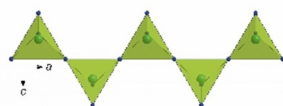## Isolated tetrahedra groups
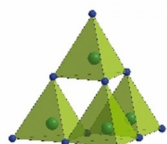
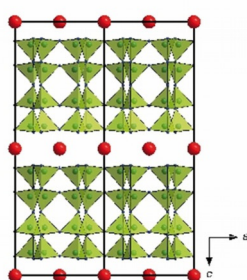adamantan like $[P_4N_{10}]^{10-}$ anion
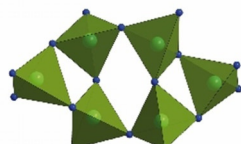
$[P_6N_{16}]^{18-}$ anion

Chains

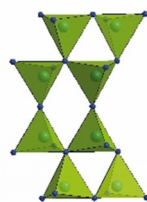Ca$_2$PN$_3$ structure with PN$_4$ tetrahedra chains

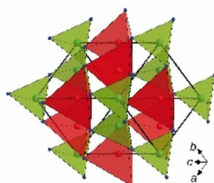*zweier* single chain

Layers

SrP$_8$N$_{14}$ structure with PN$_4$ tetrahedra layers
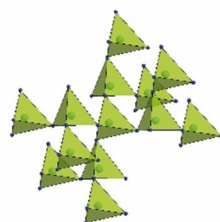
PN$_4$ tetrahedra layer

Networks

sphalerite-type superstructure of LiPN$_2$

PN$_4$ tetrahedra framework

Figure 3. Crystal structures and/or constituting PN$_4$ tetrahedra units (green) occurring in α-Li$_{10}$P$_4$N$_{10}$, β-Li$_{10}$P$_4$N$_{10}$, Li$_{18}$P$_6$N$_{16}$, Ca$_2$PN$_3$, SrP$_8$N$_{14}$, and LiPN$_2$. Ca^{2+} and Sr^{2+} cations as well as LiN$_4$ tetrahedra are depicted in red.
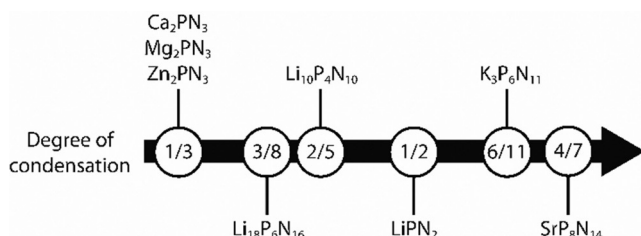

Figure 4. Ammonothermally synthesized nitridophosphates, arranged in order of their degree of condensation.

ering almost the entirely accessible range. These results show the great potential of the ammonothermal method and can pave the way for synthesis of hitherto unknown nitridophosphates using the ammonothermal approach.

Conclusions

Recently, we reported on the synthesis and crystal growth of wurtzite-type Mg$_2$PN$_3$ and Zn$_2$PN$_3$ under ammonothermal conditions, raising the question of a systematic access to nitridophosphates using supercritical NH$_3$.[17] In this contribution we report on the ammonothermal syntheses of α-Li$_{10}$P$_4$N$_{10}$, β-Li$_{10}$P$_4$N$_{10}$, Li$_{18}$P$_6$N$_{16}$, Ca$_2$PN$_3$, SrP$_8$N$_{14}$, and LiPN$_2$. Those compounds feature a degree of condensation in the range $1/3 \leq \kappa \leq 4/7$ (Figure 4), corresponding to different types of anionic tetrahedra-based substructures, such as non-condensed tetrahedra groups, chains, layers and 3D-networks. In contrast to established high-pressure techniques, the ammonothermal method requires only moderate pressures and temperatures, exemplifying the high potential of this preparative approach. Furthermore, readily available red phosphorus was introduced as a starting material in nitridophosphate syntheses, avoiding the usage of halide or sulfur-containing precursors (e.g. (PNCl$_2$)$_3$, P$_4$S$_{10}$). Using simple starting materials and yielding large sample volumes, the ammonothermal method enables more detailed characterization of material properties of nitridophosphates. Supporting fundamental research on the reaction mechanisms, intermediate species and dissolution/crystallization processes, however, might be necessary. Therefore, in situ measurements such as X-ray, NMR, or Raman techniques may provide important insights into these processes.[41,42]

Experimental Section

General

Loading of the autoclaves with solid starting materials (see below) were conducted under exclusion of oxygen and moisture in an argon-filled glovebox (Unilab, MBraun, Garching, O$_2$ < 1 ppm, H$_2$O < 1 ppm). The condensation of ammonia into the autoclaves was performed using a vacuum line ($\leq$ 0.1 Pa) with argon and ammonia (both: Air Liquide, 99.999%) supply. The gases were further purified by gas cartridges (Micro torr FT400-902 (for Ar) and MC400-702FV (for NH$_3$), SAES Pure Gas Inc., San Luis Obispo, CA, USA), providing a purity level of < 1 ppbV H$_2$O, O$_2$ and CO$_2$. The amount of condensed ammonia was detected using a mass flow meter (D-6320-DR, Bronkhorst, Ruurlo, Netherlands).

Synthesis of P$_3$N$_5$

P$_3$N$_5$ was synthesized by reaction of P$_4$S$_{10}$ (Sigma Aldrich, 99%) in a continuous flow of NH$_3$ (Air Liquid, 99.999%).[43] After saturation with NH$_3$ (4 h), the silica tube was heated with a rate of 5 K min^{-1} to 1125 K and held for 4 h. After cooling to room temperature (5 K min^{-1}), the orange product was washed with ethanol, water and acetone and dried under vacuum. Powder X-ray diffraction was used to confirm phase purity.

Synthesis of Sr(N$_3$)$_2$

Based on the work of Suhrmann and Karau,[44,45] Sr(N$_3$)$_2$ was synthesized by reaction of in situ formed diluted HN$_3$ (by passing aque-

ous NaN$_3$ (Acros Organics, 99%)) through a cation exchanger (Amberlyst 15)) with SrCO$_3$ (Sigma Aldrich, 99.995%). The HN$_3$-solution was dropped slowly into an aqueous suspension of SrCO$_3$ and stirred until the liquid phase turned completely clear. Residual SrCO$_3$ was removed by filtration and the clear filtrate was evaporated under reduced pressure (50 mbar, 40 °C). After evaporation, the product was recrystallized from acetone and dried in vacuo. PXRD and FTIR measurements were used to confirm phase purity.

Caution! Since HN$_3$ solutions are potentially explosive and the vapor is highly poisonous, special care issues are necessary.

Ammonothermal synthesis of α- and β-Li$_{10}$P$_4$N$_{10}$

For ammonothermal synthesis of α- and β-Li$_{10}$P$_4$N$_{10}$, Li$_3$N (3 mmol, 104.5 mg, Sigma–Aldrich, 99.99%) and red P (3 mmol, 92.9 mg, Merck, 99%) were ground and transferred to Ta-liners, for protection of the samples against autoclave impurities. The liners were then placed in high-temperature autoclaves (Haynes® 282®, max. 1100 K, 170 MPa, 10 mL) and sealed with a lid via flange joints using a sealing gasket (silver coated Inconel® 718 ring, GFD seals). The autoclave body and the upper part, consisting of a hand valve (SITEC) with integrated bursting disc (SITEC) and pressure transmitter (HBM P2VA1/5000 bar), are connected by an Inconel® 718 high-pressure tube.[12] The closed autoclave was evacuated and cooled to 198 K using an ethanol/liquid nitrogen mixture. Afterwards, NH$_3$ (≈4 mL) was directly condensed into the autoclaves via a pressure regulating valve. For both reactions, the autoclaves were primarily heated to 670 K within 2 h, kept at this temperature for 16 h and subsequently heated to 920 K (α-Li$_{10}$P$_4$N$_{10}$) or 1070 K (β-Li$_{10}$P$_4$N$_{10}$) within 3 h and held at this temperature for 72 h, reaching maximum pressures of 100 (α-Li$_{10}$P$_4$N$_{10}$) and 135 MPa (β-Li$_{10}$P$_4$N$_{10}$), respectively. After cooling and removal of NH$_3$, the colorless products were separated under argon, washed with EtOH and dried in vacuo.

Ammonothermal synthesis of Li$_{18}$P$_6$N$_{16}$

Li$_{18}$P$_6$N$_{16}$ was synthesized ammonothermally starting from Li$_3$N (3.75 mmol, 130.6 mg, Sigma–Aldrich, 99.99%), P$_3$N$_5$ (1.5 mmol, 244.4 mg) and NH$_3$ (≈5 mL) in a Ta-liner. Following the autoclave preparation (as described for Li$_{10}$P$_4$N$_{10}$), the vessel was heated to 670 K within 2 h, kept at this temperature for 16 h, heated to 970 K within 3 h and held at this temperature for 50 h reaching a maximum pressure of 165 MPa. After cooling and removing of NH$_3$, the colorless product was separated under argon, washed with EtOH and dried in vacuo.

Ammonothermal synthesis of Ca$_2$PN$_3$

Ca$_2$PN$_3$ was synthesized under ammonothermal conditions using an Inconel® 718 autoclave (max. 870 K, 300 MPa, 10 mL). The setup and preparation of the autoclave is analogous to the autoclaves described above. CaH$_2$ (3 mmol, 126.3 mg, Sigma–Aldrich, 99.99%), red P (1.5 mmol, 46.5 mg, Merck, 99%), NaN$_3$ (7.5 mmol, 487.5 mg, Sigma–Aldrich, 99.5%) as mineralizer and NH$_3$ (≈6.5 mL) were used as starting materials in a Ta-liner. After autoclave preparation (as described above), the reaction mixture was heated to 670 K within 2 h, held for 16 h, heated to 870 K within 2 h and kept at this temperature for 96 h, resulting in a maximum pressure of 200 MPa. The beige product was separated after cooling and ammonia removed under argon, washed with EtOH and dried in vacuo.

Ammonothermal synthesis of SrP$_8$N$_{14}$

Sr(N$_3$)$_2$ (0.375 mmol, 64.4 mg), P$_3$N$_5$ (1 mmol, 163 mg) were ground, transferred to a Ta-liner, which was placed in a Haynes® 282® autoclave. After preparation of the autoclave as described above, NH$_3$ (≈5 mL) was condensed into the autoclave. Subsequently, the autoclave was heated to 670 K within 2 h, held at this temperature for 16 h, heated to 1070 K within 3 h, and kept at this temperature for 96 h, reaching a maximum pressure of 170 MPa. After cooling and removal of NH$_3$, the colorless product was isolated in air, washed with 1 M HCl and dried at 370 K.

Ammonothermal synthesis of LiPN$_2$

For the synthesis of LiPN$_2$ in supercritical ammonia, Li (10 mmol, 69.4 mg, Alfa Aesar, 99%) and red P (7.5 mmol, 232.3 mg, Merck, 99%) were transferred in a Ta-liner and placed in a Haynes® 282® autoclave. After preparation of the autoclave as described above, approximately 4 mL NH$_3$ were added. The reaction mixture was heated to 670 K within 2 h, held for 16 h, heated to 1070 K within 3 h and kept at this temperature for 96 h, resulting in maximum pressures of 135 MPa. After cooling and elimination of NH$_3$, the isolated colorless product was washed with 1 M HCl and dried at 370 K.

Powder X-ray diffraction

The purified products were filled and sealed in glass capillaries (0.3–0.5 mm diameter, 0.01 mm wall thickness, Hilgenberg GmbH). A Stoe STADI P diffractometer with Cu-K$_{\alpha1}$ radiation ($\lambda = 1.5406$ Å), Ge(111) monochromator and Mythen 1 K detector in Debye–Scherrer geometry was used for data collection. TOPAS was used for Rietveld refinement.[46]

Scanning electron microscopy

A Dualbeam Helios Nanolab G3 UC (FEI) scanning electron microscope, equipped with an EDX detector (X-Max 80 SDD, Oxford instruments) was used for EDX measurements. For this purpose, the samples were placed on adhesive carbon pads and coated with a conductive carbon film using a high-vacuum sputter coater (BAL-TEC MED 020, Bal Tec A).

FTIR spectroscopy

A FTIR-IFS 66 v/S spectrometer (Bruker) was used for recording of IR spectra of air-sensitive samples. The samples were mixed with KBr (Acros Organics, 99%) under argon and pressed into a pellet. The spectra were measured in the range of 400–4000 cm^{-1} and evaluated by OPUS.[47]

A FTIR spectrum of LiPN$_2$ was recorded on a Perkin–Elmer BX II FTIR spectrometer equipped with a DuraSampler Diamond ATR (attenuated total reflection) unit under exposure to air.

Conflict of interest

The authors declare no conflict of interest.

[1] H. Jacobs, R. Juza, *Z. Anorg. Allg. Chem.* **1969**, *370*, 254–261.
[2] R. Juza, H. Jacobs, *Angew. Chem. Int. Ed. Engl.* **1966**, *5*, 247; *Angew. Chem.* **1966**, *78*, 208.
[3] H. Jacobs, E. von Pinkowski, *J. Less-Common Met.* **1989**, *146*, 147–160.
[4] J. Häusler, W. Schnick, *Chem. Eur. J.* **2018**, *24*, 11864–11879.
[5] T. Richter, R. Niewa, *Inorganics* **2014**, *2*, 29–78.
[6] R. Dwiliński, R. Doradziński, J. Garczyński, L. Sierzputowski, R. Kucharski, M. Zając, M. Rudziński, R. Kudrawiec, W. Strupiński, J. Misiewicz, *Phys. Status Solidi A* **2011**, *208*, 1489–1493.
[7] S. Pimputkar, S. Kawabata, J. S. Speck, S. Nakamura, *J. Cryst. Growth* **2014**, *403*, 7–17.
[8] W. Jiang, D. Ehrentraut, J. Cook, D. S. Kamber, R. T. Pakalapati, M. P. D'Evelyn, *Phys. Status Solidi B* **2015**, *252*, 1069–1074.
[9] J. B. Shim, G. H. Kim, Y. K. Lee, *J. Cryst. Growth* **2017**, *478*, 85–88.
[10] J. Hertrampf, P. Becker, M. Widenmeyer, A. Weidenkaff, E. Schlücker, R. Niewa, *Cryst. Growth Des.* **2018**, *18*, 2365–2369.
[11] J. Häusler, R. Niklaus, J. Minár, W. Schnick, *Chem. Eur. J.* **2018**, *24*, 1686–1693.
[12] J. Häusler, S. Schimmel, P. Wellmann, W. Schnick, *Chem. Eur. J.* **2017**, *23*, 12275–12282.
[13] J. Häusler, L. Neudert, M. Mallmann, R. Niklaus, A.-C. L. Kimmel, N. S. A. Alt, E. Schlücker, O. Oeckler, W. Schnick, *Chem. Eur. J.* **2017**, *23*, 2583–2590.
[14] M. Mallmann, R. Niklaus, T. Rackl, M. Benz, T. G. Chau, D. Johrendt, J. Minár, W. Schnick, *Chem. Eur. J.* **2019**, *25*, 15887–15895.
[15] N. Cordes, W. Schnick, *Chem. Eur. J.* **2017**, *23*, 11410–11415.
[16] H. Jacobs, R. Nymwegen, *Z. Anorg. Allg. Chem.* **1997**, *623*, 429–433.
[17] M. Mallmann, C. Maak, R. Niklaus, W. Schnick, *Chem. Eur. J.* **2018**, *24*, 13963–13970.
[18] S. D. Kloß, W. Schnick, *Angew. Chem. Int. Ed.* **2019**, *58*, 7933–7944; *Angew. Chem.* **2019**, *131*, 8015–8027.
[19] H. Jacobs, R. Nymwegen, S. Doyle, T. Wroblewski, W. Kockelmann, *Z. Anorg. Allg. Chem.* **1997**, *623*, 1467–1474.
[20] H. Jacobs, S. Pollok, F. Golinski, *Z. Anorg. Allg. Chem.* **1994**, *620*, 1213–1218.

[21] H. Jacobs, F. Golinski, *Z. Anorg. Allg. Chem.* **1994**, *620*, 531–534.
[22] F. Golinski, H. Jacobs, *Z. Anorg. Allg. Chem.* **1995**, *621*, 29–33.
[23] W. Schnick, J. Luecke, *J. Solid State Chem.* **1990**, *87*, 101–106.
[24] W. Schnick, J. Lücke, *Z. Anorg. Allg. Chem.* **1990**, *588*, 19–25.
[25] W. Schnick, U. Berger, *Angew. Chem. Int. Ed. Engl.* **1992**, *30*, 830–831; *Angew. Chem.* **1991**, *103*, 857–858.
[26] E. M. Bertschler, C. Dietrich, T. Leichtweiß, J. Janek, W. Schnick, *Chem. Eur. J.* **2018**, *24*, 196–205.
[27] W. Schnick, V. Schultz-Coulon, *Angew. Chem. Int. Ed. Engl.* **1993**, *32*, 280–281; *Angew. Chem.* **1993**, *105*, 308–309.
[28] S. D. Kloß, N. Weidmann, R. Niklaus, W. Schnick, *Inorg. Chem.* **2016**, *55*, 9400–9409.
[29] V. Schultz-Coulon, W. Schnick, *Z. Anorg. Allg. Chem.* **1997**, *623*, 69–74.
[30] S. Wendl, W. Schnick, *Chem. Eur. J.* **2018**, *24*, 15889–15896.
[31] E.-M. Bertschler, C. Dietrich, J. Janek, W. Schnick, *Chem. Eur. J.* **2017**, *23*, 2185–2191.
[32] S. D. Kloß, W. Schnick, *Angew. Chem. Int. Ed.* **2015**, *54*, 11250–11253; *Angew. Chem.* **2015**, *127*, 11402–11405.
[33] J. M. Sullivan, *Inorg. Chem.* **1976**, *15*, 1055–1059.
[34] F. Friedrichs, *J. Am. Chem. Soc.* **1913**, *35*, 1866–1883.
[35] J. Hertrampf, N. S. A. Alt, E. Schlücker, R. Niewa, *Eur. J. Inorg. Chem.* **2017**, 902–909.
[36] H. Jacobs, U. Fink, *J. Less-Common Met.* **1979**, *63*, 273–286.
[37] F. Golinski, H. Jacobs, *Z. Anorg. Allg. Chem.* **1994**, *620*, 965–968.
[38] H. Jacobs, R. Kirchgässner, *Z. Anorg. Allg. Chem.* **1990**, *581*, 125–134.
[39] The terms *dreier* rings, *vierer* rings and *zweier* single chain were coined by Liebau and are derived from the German words „dreier, vierer and zweier"; a *dreier* ring comprises three tetrahedra centers, a *vierer* ring four tetrahedra centers, a *zweier* chain can be described as two polyhedra within one repeating unit of the linear part of the chain.
[40] F. Liebau, *Structural Chemistry of Silicates*, Springer, Berlin, **1985**, 80.
[41] S. Schimmel, M. Lindner, T. G. Steigerwald, B. Hertweck, T. M. M. Richter, U. Künecke, N. S. A. Alt, R. Niewa, E. Schlücker, P. J. Wellmann, *J. Cryst. Growth* **2015**, *418*, 64–69.
[42] T. G. Steigerwald, J. Balouschek, B. Hertweck, A.-C. L. Kimmel, N. S. A. Alt, E. Schlücker, *J. Supercrit. Fluids* **2018**, *134*, 96–105.
[43] A. Stock, B. Hoffmann, *Ber. Dtsch. Chem. Ges.* **1903**, *36*, 314–319.
[44] R. Suhrmann, K. Clusius, *Z. Anorg. Allg. Chem.* **1926**, *152*, 52–58.
[45] F. W. Karau, *Dissertation*, Ludwig-Maximilians-Universität München (Germany) **2007**.
[46] A. Coelho, *TOPAS Academic*, Version 6, Coelho Software, Brisbane (Australia), **2016**.
[47] *OPUS/IR*, Brucker Analytik GmbH, Karlsruhe, **2000**.